Available online at www.sciencedirect.com
ScienceDirect
International Journal of Thermal Sciences 48 (2009) 521–534
International Journal of Thermal Sciences
www.elsevier.com/locate/ijts

Multiple steady states in a porous enclosure partially heated and fully salted from below

Z. Alloui [a,*,1], L. Dufau [a], H. Beji [b], P. Vasseur [b]

[a] *Ecole Polytechnique, Université de Montréal, C.P. 6079, Succ. "Centre ville", Montréal, Québec, H3C 3A7, Canada*
[b] *Laboratoire des Technologies Innovantes, Université Jules Vernes d'Amiens, rue des Facultés le Bailly, 800025 Amiens Cedex, France*

Received 14 January 2008; received in revised form 5 May 2008; accepted 18 May 2008

Available online 16 June 2008

Abstract

The Darcy model with the Boussinesq approximation is used to study natural convection in a porous medium saturated by a binary fluid. The geometry considered is a square cavity whose portion of the bottom surface is isothermally heated, the upper surface is cooled at a constant temperature and all other surface are adiabatic. The solutal buoyancy forces are assumed to be induced by the imposition of uniform concentration on the upper and lower boundaries. The governing parameters for the problem are the thermal Rayleigh number, R_T, the Lewis number, Le, the buoyancy ratio, φ, the dimensionless length of the bottom plate, B_T, the aspect ratio of the cavity A, the normalized porosity of the porous medium, ε, and the relative position of the heating element with respect to the vertical centerline of the cavity, δ_T. Two main convective modes are studied, namely single and double-cell convection, and their features are described. Also the possible existence of tricellular flows is demonstrated. Maximum streamfunction and global Nusselt and Sherwood number are presented as functions of the external parameters. The existence of up to three steady-state solutions for a given set of the governing parameters is demonstrated.

Keywords: Natural convection; Porous media; Double diffusion; Partial heating

1. Introduction

Natural convection in porous media saturated by a binary mixture is of importance in many natural and industrial problems. Such applications include ground water pollution, geothermal systems, crude oil production, storage of energy, and so on. A comprehensive review of the natural convection due to combined thermal and solutal driving forces was conducted by Ostrach [1], Viskanta et al. [2] and Nield and Bejan [3].

Much of the early published works regarding the problem of combined heat and mass transfer concerns the problem of the onset of convection in a horizontal porous layer heated and salted from below [4–8]. On the basis of the linear stability theory, the onset of convection of stationary and oscillatory convection was derived by these authors for various thermal and solutal boundary conditions. A few studies have also been reported concerning the regime of finite amplitude within a porous medium subjected to vertical gradient of heat and solute. Trevisan and Bejan [9] studied numerically and theoretically the mass transfer resulting from high convection in a porous medium heated from below. Their results indicate the existence of different scaling laws for the dependence of the Nusselt number versus the Rayleigh and Lewis numbers. Thermo-solutal bifurcation phenomena in porous enclosures subject to vertical temperature and concentration gradients has been studied analytically and numerically by Mamou and Vasseur [10]. The onset and development of convection was investigated using both linear and nonlinear perturbation theories. The existence of multiple solutions and the occurrence of travelling waves was demonstrated. The onset of convection in a horizontal porous layer has been investigated by Sovran et al. [11]. The Soret effect, for which species gradients are not due to the imposition of solutal boundary conditions but result rather from temperature gradients, was considered by these authors. Recently, double-diffusive and Soret-induced convection in a shallow horizontal

* Corresponding author.
E-mail address: zineddine.alloui@polymtl.ca (Z. Alloui).
[1] http://www.meca.polymtl.ca/convection

1290-0729/$ – see front matter
doi:10.1016/j.ijthermalsci.2008.05.008

Nomenclature

A	aspect ratio of the cavity, (L'/H')
B_T	dimensionless length of heat source, (d'_T/H')
C	mass fraction
D	mass diffusivity of species ..... m^2/s
g	gravitational acceleration ..... m/s^2
H'	side of the square cavity ..... m
k	thermal conductivity ..... $W/(m\,K)$
K	permeability of saturated porous medium ..... m^2
Le	Lewis number, (α/D)
N	mass fraction
N_0	reference mass fraction
ΔN	characteristic mass fraction difference, $(N_H - N_C)$
Nu	Nusselt number, Eq. (13)
R_T	thermal Rayleigh number, $(g\beta'_T K \Delta T' H'/\nu\alpha)$
S	normalized mass fraction, $N/\Delta N$
Sh	Sherwood number, Eq. (14)
t	dimensionless time, $t'\alpha/H'^2$
T	dimensionless temperature, $(T' - T'_C)/\Delta T'$
$\Delta T'$	characteristic temperature difference, $(T'_H - T'_C)$
u	dimensionless velocity in x direction, $(u'H'/\alpha)$
v	dimensionless velocity in y direction, $(v'H'/\alpha)$
x	dimensionless coordinate axis, (x'/H')
y	dimensionless coordinate axis, (y'/H')

Greek symbols

α	thermal diffusivity ..... m^2/s
β_N	concentration expansion coefficient
β'_T	thermal expansion coefficient ..... K^{-1}
ε	normalized porosity of the porous medium, ϕ/σ
δ_T	dimensionless position of heat source, δ'_T/H'
ν	kinematic viscosity of fluid ..... m^2/s
φ	buoyancy ratio, $(\beta_N \Delta N/\beta'_T \Delta T')$
ρ	density of fluid ..... kg/m^2
$(\rho C)_f$	heat capacity of the fluid ..... W/K
$(\rho C)_p$	heat capacity of the saturated porous medium ..... W/K
σ	heat capacity ratio, $(\rho C)_p/(\rho C)_f$
ϕ	porosity of the porous medium
Ψ	dimensionless streamfunction, Ψ'/α

Subscript

0	reference state

Superscript

$'$	refers to dimensional variable

layer subject to vertical gradients of temperature and solute has been studied by Bahloul et al. [12]. The thresholds for finite-amplitude, oscillatory and monotonic convection instabilities were determined in terms of the governing parameters. Numerical solutions are presented for a wide range of the governing parameters.

A literature review shows that relatively little work is available on the case of natural convection in a porous cavity, driven by localized heating from below. The theoretical work, for this configuration has been pioneered by Elder [13,14]. Numerical results were reported by El-Khatib and Prasad [15] for the case of a square cavity, in the presence of stable linear gradients. Detailed flow and temperature field solutions are discussed for various values of thermal stratification ratio. Multiple steady states in a confined porous medium, with localized heating from below have been reported numerically by Robillard et al. [16]. For a square enclosure unicellular and bicellular symmetrical circulations have been studied for various sizes and positions of the heated element.

All the above studies are concerned with the case of single diffusive convection in a porous cavity with discrete heat source from below. The problem of double diffusive natural convection within a porous cavity with discrete heat and mass sources has been considerably less studied, despite its width range of applications in many engineering fields. Bourich et al. [17] studied numerically the existence of multiple solutions in a porous enclosure partially heated from below and differentially salted. It was demonstrated that the multiplicity of solution obtained in pure thermal convection vanishes in the presence of horizontal solutal gradients when critical conditions, depending on the Rayleigh and Lewis number, are reached. The problem of double diffusive natural convection within a vertical porous enclosure with localized heating and salting element from one side, subjected to constant heat and mass fluxes, has been studied numerically by Di Liu et al. [18]. The same problem was reconsidered by Zhao et al. [19] for the case when the localized element is maintained at constant temperature and concentration. A large range of buoyancy ratios was considered by these authors in order to illustrate the flow structure transitions and flow reversals. The existence of multiple steady flows in confined gaseous double diffusion with discrete thermosolutale sources has been investigated by Zhao et al. [20]. The same authors [21] also considered the double diffusive natural convection induced by discrete thermosolutale sources in a porous enclosure.

The present paper investigates numerically double diffusive natural convection within a porous enclosure with localized heating and salting from below. The paper is organized as follows. First, the physical model and mathematical formulation of the problem is presented. Then, some relevant details of the computational method utilized to solve the full governing equations are presented. Finally, the results from the numerical computations are discussed and conclusions are drawn.

2. Mathematical formulation

Consider a square cavity of side H' filled with an isotropic porous medium saturated by a binary mixture (see Fig. 1). All the boundaries are impermeable, the vertical walls are in-

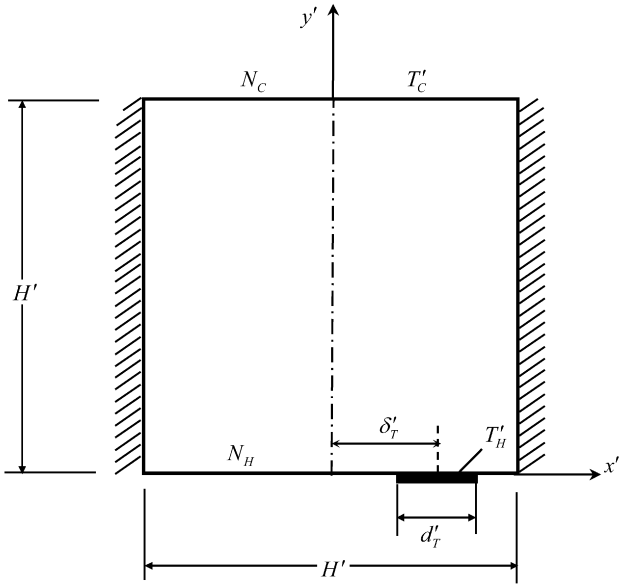

Fig. 1. Geometry and boundary conditions of the problem.

sulated, and the top horizontal wall is kept at uniform temperature T'_C and concentration N_C. The bottom wall is maintained at uniform concentration N_H ($> N_C$) while an element of length d'_T is maintained at a temperature T'_H ($> T'_C$), the rest of the horizontal boundary being insulated. The distance between the center of the heating element and the vertical center line of the cavity is δ'_T. The porous medium is considered to be homogeneous and isotropic and in local thermal and compositional equilibrium with the fluid. The binary mixture is assumed to be Newtonian and to satisfy the Boussinesq approximation. The density variation with temperature and concentration is described by the state equation $\rho = \rho_0[1 - \beta'_T(T' - T'_0) - \beta_N(N - N_0)]$ where ρ_0 is the fluid mixture density at temperature $T' = T'_0$ and mass fraction $N = N_0$ and β'_T and β_N are thermal and concentration expansion coefficients, respectively. The subscript 0 refers to a reference state.

The phenomenological equations relating the fluxes of heat $\vec{Q}'$ and matter $\vec{J}'$ to the thermal and solute gradients present in a binary fluid mixture are given by [22]:

$$\vec{Q}' = -k\nabla T'$$
$$\vec{J}' = -\rho D\nabla N \tag{1}$$

where k and D are the thermal conductivity and the mass diffusivity of species through the fluid saturated porous medium. In the above equations the interactions between the thermal and concentration gradients, known as the Soret and Dufour effects, are neglected.

The equations expressing conservation of momentum, energy and species are given by

$$\nabla^2\Psi' = -\frac{gK\beta'_T}{\nu}\frac{\partial}{\partial x'}\left(T' + \frac{\beta_N}{\beta'_T}N\right) \tag{2}$$

$$(\rho C)_{\mathrm{p}}\frac{\partial T'}{\partial t'} + (\rho C)_{\mathrm{f}}\mathbf{V}'\cdot\nabla T' = k\nabla^2 T' \tag{3}$$

$$\phi\frac{\partial N}{\partial t'} + \mathbf{V}'\cdot\nabla N = D\nabla^2 N \tag{4}$$

where $\mathbf{V}'$ is the Darcy velocity, g the gravitational acceleration, ν the kinematic viscosity, $(\rho C)_{\mathrm{p}}$ and $(\rho C)_{\mathrm{f}}$ are respectively the heat capacity of the saturated porous medium and the fluid, ϕ the porosity of the porous matrix, t' the time and Ψ' the stream-function. As usual, $u' = \partial\Psi'/\partial y'$ and $v' = -\partial\Psi'/\partial x'$, such that the conservation of mass is satisfied.

The boundary conditions applied on the system are:

$$x' = \pm L'/2, \quad \Psi' = 0, \quad \partial T'/\partial x' = \partial N/\partial x' = 0$$
$$y' = H', \quad \Psi' = 0, \quad T' = T'_C, \quad N = N_C$$
$$y' = 0, \quad \Psi' = 0, \quad N = N_H$$
$$\text{on surface } d'_T\text{: } T' = T'_H, \quad \text{everywhere else: } \partial T'/\partial y' = 0 \tag{5}$$

The dimensionless variables (primed quantities are dimensional) are defined as follows

$$(x, y) = (x', y')/H', \qquad (u, v) = (u', v')H'/\alpha$$
$$t = t'\alpha/H'^2, \qquad \varepsilon = \phi/\sigma$$
$$T = (T' - T'_C)/\Delta T', \qquad S = (N - N_C)/\Delta N$$
$$\Psi = \Psi'/\alpha \tag{6}$$

where $\Delta T' = (T'_H - T'_C)$, $\Delta N = (N_H - N_C)$ and $\sigma = (\rho C)_{\mathrm{p}}/(\rho C)_{\mathrm{f}}$ is the heat capacity ratio.

In terms of the above definitions, the dimensionless governing equations are given by

$$\nabla^2\Psi = -R_T\left(\frac{\partial T}{\partial x} + \varphi\frac{\partial S}{\partial x}\right) \tag{7}$$

$$\frac{\partial T}{\partial t} + u\frac{\partial T}{\partial x} + v\frac{\partial T}{\partial y} = \nabla^2 T \tag{8}$$

$$\varepsilon\frac{\partial S}{\partial t} + u\frac{\partial S}{\partial x} + v\frac{\partial S}{\partial y} = \frac{1}{Le}\nabla^2 S \tag{9}$$

The corresponding dimensionless boundary conditions are given by

$$x = \pm A/2, \quad \Psi = 0, \quad \partial T/\partial x = \partial S/\partial x = 0$$
$$y = 1, \quad \Psi = 0, \quad T = 0, \quad S = 0$$
$$y = 0, \quad \Psi = 0, \quad S = 1$$
$$\text{on surface } B_T\text{: } T = 1, \quad \text{everywhere else: } \partial T/\partial y = 0 \tag{10}$$

In addition to the boundary conditions, it is also necessary to specify some initial conditions at time $t = 0$. This is done by using a "stirred" flow as the initial condition of the evolutive problem; this is written as follows:

$$\Psi = \Psi_{\mathrm{p}}\sin m\pi x\sin n\pi y \tag{11}$$

where Ψ_{p} is the amplitude of the initial perturbation and m and n are wave-numbers of the initial disturbance.

From the above equations it is seen that the present problem is governed by the thermal Rayleigh number R_T, the buoyancy ratio φ, the Lewis number Le, the normalized porosity ε and the cavity aspect ratio A, the dimensionless length of thermal source B_T and the position of thermal source δ_T. These parameters are given by

Table 1
Dimensionless heat transfer Q_C for $A = 1$, $\delta_T = 0$ and various values of B_T

B_T	1.0	0.9	0.8	0.7	0.6	0.5	0.4	0.3	0.2
Q_C	1.000	0.997	0.985	0.966	0.939	0.902	0.859	0.803	0.733

$$R_T = \frac{g\beta'_T K \Delta T' H'}{\alpha \nu}, \quad \varphi = \frac{\beta_N \Delta N}{\beta'_T \Delta T'}, \quad Le = \frac{\alpha}{D}, \quad A = \frac{L'}{H'}$$

$$\varepsilon = \frac{\phi}{\sigma}, \quad B_T = \frac{d'_T}{H'}, \quad \delta_T = \frac{\delta'_T}{H'} \tag{12}$$

In the present study the intensity of the thermal and solutal buoyancy forces are expressed in terms of the parameters R_T and φ. It is noted that for $\varphi > 0$ both the thermal and solutal buoyancy forces are cooperative while for $\varphi < 0$ they are opposing each other.

The heat and mass transfer rates on the surfaces of heat and mass sources are given by the Nusselt number Nu and Sherwood number Sh

$$Nu = \frac{1}{Q_C} \int_{-A/2}^{A/2} \left. \frac{\partial T}{\partial y} \right|_{y=1} dx \tag{13}$$

$$Sh = \frac{1}{J_C} \int_{-A/2}^{A/2} \left. \frac{\partial S}{\partial y} \right|_{y=1} dx \tag{14}$$

where Q_C and J_C are the pure diffusion dimensionless heat and mass transfer, respectively.

In the present study the values of Q_C and J_C, which depend upon parameters A, B_T, B_N, δ_T and δ_N, were obtained from the numerical code described in the following section, for the condition $R_T = 0$ (pure conduction). Table 1 illustrates typical results obtained for Q_C in terms of the dimensionless length of the heated element B_T when $\delta_T = 0$.

3. Numerical solution

The numerical solution of governing equations (7)–(9) with specified boundary conditions equations (10), is obtained using the SIMPLER algorithm (Patankar [23]). The control-volume formulation used in the algorithm ensures continuity of the convective and diffusive fluxes as well as overall momentum energy and solute conservation. The discretized equations are derived using the central differences for spatial derivatives and backward differences for time derivatives. The governing equations are converted into a system of algebraic equations through integration over each control volume. The algebraic equations are solved by a line-by-line iterative method. The method sweeps the domain of integration along the x and y-axes and uses tri-diagonal matrix inversion to solve the resulting system of equations. The streamfunction equation (7) is solved by SOR (Successive Over-Relaxation) method. Starting from given specified initial values of variables, the dimensionless time step which yielded convergence for the majority of cases was $\Delta t = 10^{-4}$. The iterative process, employed to find the streamfunction, temperature and concentration fields, was repeated until the following convergence criterion was satisfied

$$\frac{\sum_i \sum_j (\Phi_{i,j}^{\text{new}} - \Phi_{i,j}^{\text{old}})}{\sum_i \sum_j \Phi_i^{\text{new}}} \leqslant 10^{-6} \tag{15}$$

where Φ stand for Ψ, T and S. The subscripts i and j denote grid locations in the (x, y) plane. A further decrease of the convergence criteria 10^{-6} does not cause any significant change in the final results. Besides the usual control, the accuracy of computations was controlled using energy and mass fraction conservation within the system.

A nonuniform mesh structure was employed, the nodal point being skewed in x- and y-direction to obtain a greater concentration of points near the solid boundaries. Numerical tests, using various mesh sizes, were done for the same conditions in order to determine the best compromise between accuracy of the results and computer time. A mesh size of 81×81 was adopted for most of the cases considered in this study. The accuracy of the code was checked, modifying the thermal and solutal boundary conditions, to reproduce the results reported in the literature for the case of double-diffusive convection within a square cavity differentially heated and salted from the vertical sides. Good agreement can be seen from Table 2 with a maximum deviation of about 3.75%

Table 2
Validation of the numerical code, for $A = 1$, $Le = 100$, $\varphi = 0$, in terms of Nu and Sh

	$R_T = 100$		$R_T = 1000$	
	Nu	Sh	Nu	Sh
Goyeau et al. [26]	3.11	41.53	13.47	140.65
Zhao et al. [19]	3.09	42.84	13.45	145.96
Present work	3.10	43.15	13.69	142.75

4. Results and discussion

The present problem is governed by nine parameters, namely $R_T, \varphi, Le, A, \varepsilon, B_T, B_N, \delta_T$ and δ_N. Because of the abundance of parameters the study is limited to a square cavity ($A = 1$). In the actual computations R_T is set equal to 200, Le is fixed at 10 and $\varepsilon = 1$. In most of the results presented here the size of the heated element is maintained at $B_T = 0.4$ and two different positions are considered, namely $\delta_T = 0$ and 0.15.

Typical numerical results are presented in Figs. 2(a)–(f) for $R_T = 200$ and $\varphi = 0$. Positive and negative streamlines Ψ correspond to counterclockwise and clockwise circulations, respectively. In all these graphs, the increments between adjacent streamlines are $\Delta\Psi = (\Psi_{\max} - \Psi_{\min})/10$. Past studies on natural double-diffusive convection in a cavity fully heated and salted from bottom have demonstrated the existence of multiple solutions, for a given set of the governing parameters (see for instance Mamou et al. [24]). This behaviour results from the nonlinearity of the governing equations. When multiple steady states are possible, the final steady state achieved is determined by the initial conditions chosen to initiate the numerical procedure. For a classical Bénard situation, i.e. when the cavity

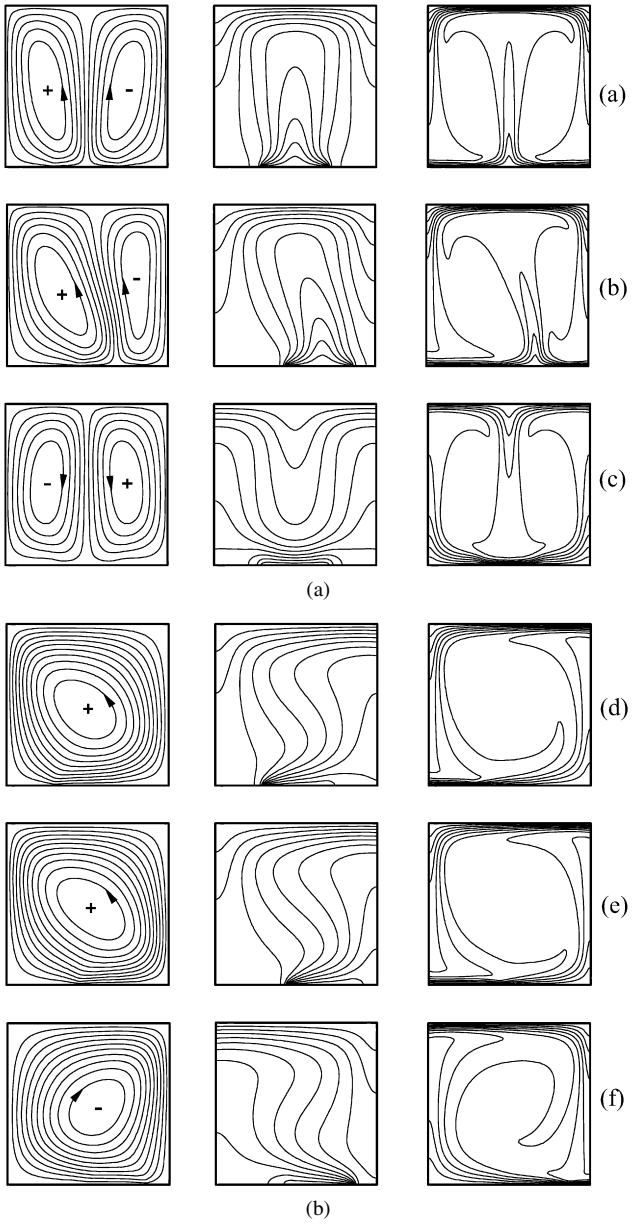

Fig. 2. Steady-state streamlines for $\varphi = 0$, $B_T = 0.4$ and (a) $\delta_T = 0$, $\Psi_{\min} = -5.57$, $\Psi_{\max} = 5.57$, (b) $\delta_T = 0.15$, $\Psi_{\min} = -4.40$, $\Psi_{\max} = 6.17$, (c) $\delta_T = 0$, $\Psi_{\min} = -4.40$, $\Psi_{\max} = 4.40$, (d) $\delta_T = 0$, $\Psi_{\min} = 0$, $\Psi_{\max} = 8.65$, (e) $\delta_T = 0.15$, $\Psi_{\min} = 0$, $\Psi_{\max} = 8.64$, (f) $\delta_T = 0.15$, $\Psi_{\min} = -8.34$, $\Psi_{\max} = 0$.

is fully heated by the bottom ($B_T = 1$) the numerical results, not presented here, indicate that above a critical Rayleigh number, the flow field consists in a single cell rotating indifferently clockwise or counterclockwise. Thus, starting with the rest state as initial values, the direction of rotation of the cell is not imposed by the physics of the problem but rather is induced by the round-off errors generated in the numerical computation. However, starting with appropriate initial conditions, a flow pattern indicating the existence of two counterrotating cells is also possible for the same set of governing parameters [16].

When the cavity is partially heated by the bottom both unicellular and bicellular flow patterns are also possible. In the present study, the convective motion will be referred to as natural flow whenever the fluid is ascendant above the heated element. On the other hand the convective pattern will be called antinatural when the fluid is descendant above the heated element. Fig. 2(a) illustrates the natural flow pattern obtained when the heated segment is centrally located ($\delta_T = 0$). Thus, starting with the rest state as initial conditions, the numerical code predicts the formation of two cells. The direction of the rotation of the cells is imposed by the physics of the problem, the fluid being ascendant above the heated element. This type of flow, according to the above convection, is thus a natural flow. When the heated element is moved ($\delta_T = 0.15$), Fig. 2(b) indicates that the same bicellular flow pattern is obtained. However, as expected, the symmetry of the flow observed in Fig. 2(a), is now destroyed. Antinatural flow patterns will be now discussed. Fig. 2(c) shows a bicellular flow pattern obtained in the case of a centrally heated segment. It is noted that now the fluid motion above the heated element is not ascendant but rather moves down toward it. To obtain this type of flow it is necessary to choose carefully the initial conditions, and in particular the number of cells and their initial sense of rotation. This was done by starting the initial conditions of the evolutive problem with the arbitrary convective flow defined by Eq. (11). This condition allows initiation of m convective rolls in the x direction with alternating clockwise and counterclockwise rotation. Unicellular flow patterns will be now considered. Fig. 2(d) shows the case of a single cell flow over a centrally located heated segment. Naturally, due to the symmetry of the problem, the cell can rotate indifferently in either direction. The sense of rotation depends only on the initial flow circulation used to initiate the numerical procedure. As the position of the heated element is moved to the right it is observed from Fig. 2(e) that an anticlockwise unicellular natural convective cell is possible. On the other hand, the clockwise circulation of Fig. 2(f) corresponds to an antinatural flow. When both natural and antinatural flows are possible, for a given set of parameters, the maximum strength of convection Ψ_{ext} is always associated with the natural flow. This point is illustrated by Figs. 2(e) and 2(f), for unicellular flow patterns and Figs. 2(a) and 2(c) for bicellular flow patterns. Finally, it is noted that the existence of the natural and antinatural, unicellular and bicellular, flow patterns depicted in Figs. 2(a)–(f) depends strongly upon the governing parameters of the problem. This point will be discussed below in more details.

Fig. 3(a) illustrates the effect of buoyancy ration φ on the maximum and minimum streamfunction $\Psi_{\max}$ and $\Psi_{\min}$, respectively, in the case of a centrally located heated segment ($\delta_T = 0$). All the curves presented in this graph were obtained starting the numerical solution with the flows already obtained in Fig. 2, for a centrally located heated segment, as initial conditions. Thus three branches corresponding to the natural and antinatural bicellular flows, Figs. 2(a) and 2(c), respectively, and the unicellular cell, Fig. 2(d) were obtained. For each curve, upon increasing or decreasing φ and using the last numerical solution as initial conditions for the next value of φ, the resulting curves were found to follow the hysteresis loops indicated by the arrows. Starting with the bicellular natural solution, Fig. 2(a), it is observed that the resulting branch exists for all

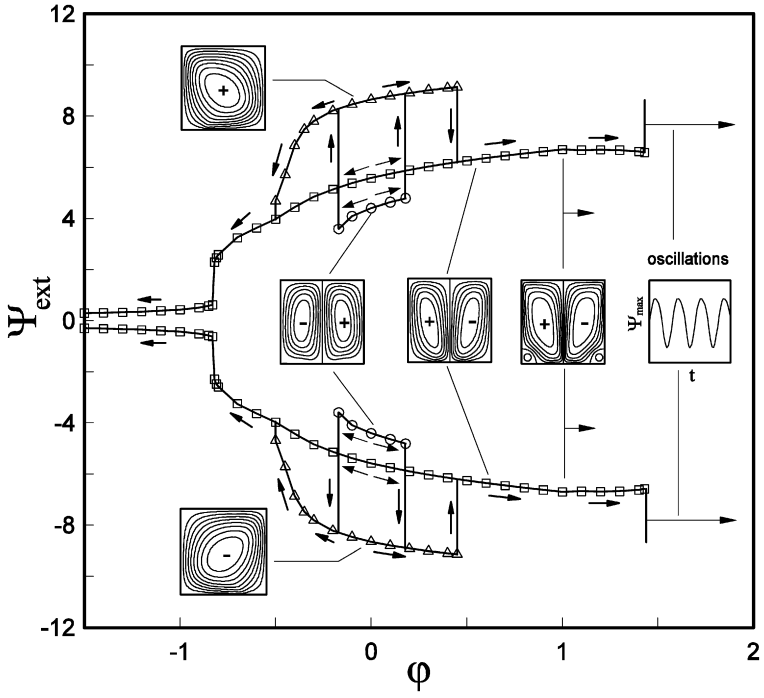

(a)

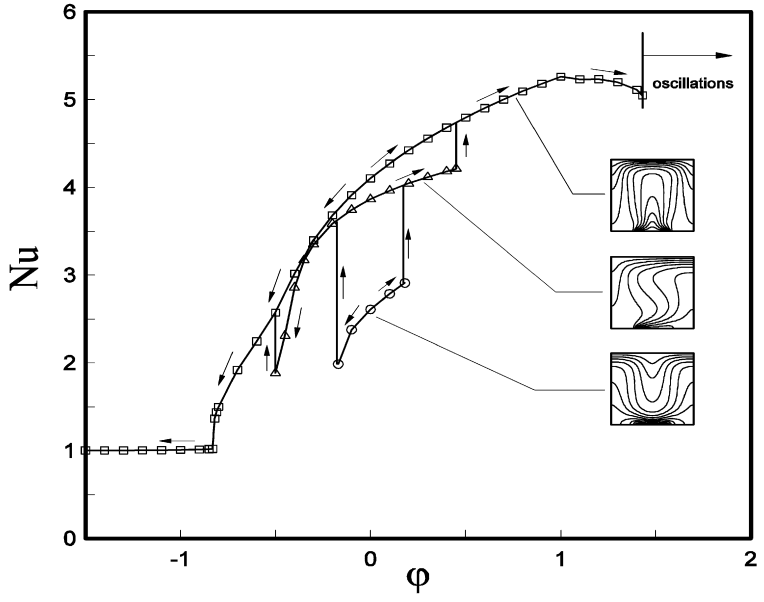

(b)

Fig. 3. Effect of buoyancy ratio φ on (a) Ψ_{ext}, (b) Nu, (c) Sh, for $B_T = 0.4$ and $\delta_T = 0$; △: 1 cell, □: 2 natural cells, ○: 2 antinatural cells.

the values of φ considered here. Upon increasing the value of φ from zero to 1.43, the intensity of the flow is notably enhanced since the thermal and solutal buoyancy forces are cooperative. As a result, as depicted in Figs. 3(b) and 3(c), the heat and mass transfer are also considerably promoted. The reverse situation is observed, upon decreasing the value of φ, an almost rest state being reached ($Nu \to 1$, $Sh \to 1$) for values of $\varphi \leqslant -0.83$. It is noted that the vertical density gradients, induced by the lower salted boundary ($B_N = 1$), are destabilizing for $\varphi > 0$, but stabilizing for $\varphi < 0$. The upper (lower) natural unicellular anticlockwise (clockwise) circulation branch will be now discussed. Starting from the condition $\varphi = 0$ it is found, that upon increasing the value of φ, it is possible to maintain this flow structure up to $\varphi \simeq 0.45$. Above this value, the unicellular flow patterns branch transits towards the bicellular natural flow pattern branch. Similarly, upon decreasing φ below 0, it is found that the critical buoyancy ratio above which the unicellular regime can be maintained is equal to -0.50. Below this value, only the bicellular natural flow pattern was found to exist. The transition between these two flow structures is exemplified in Fig. 4. For $\varphi = -0.30$ the flow is unicellular and the circulation anticlockwise, as illustrated in Fig. 4(a). As the value of

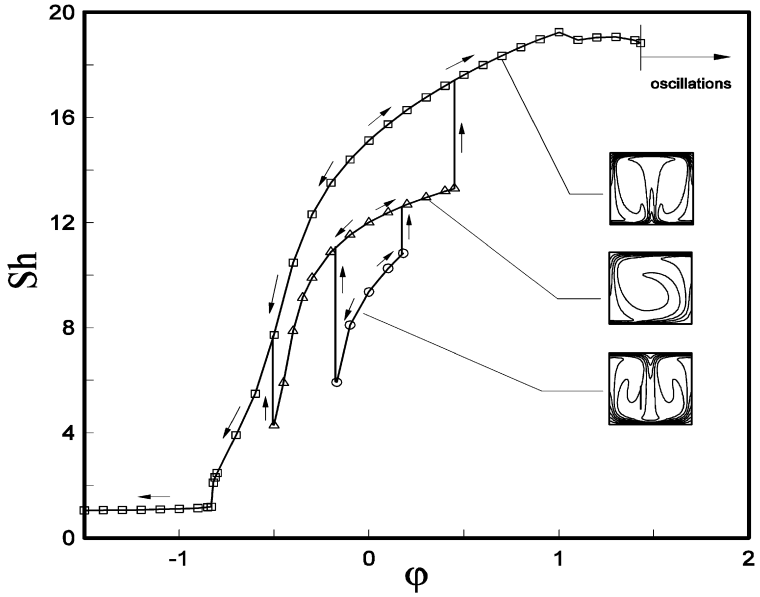

(c)

Fig. 3. (Continued).

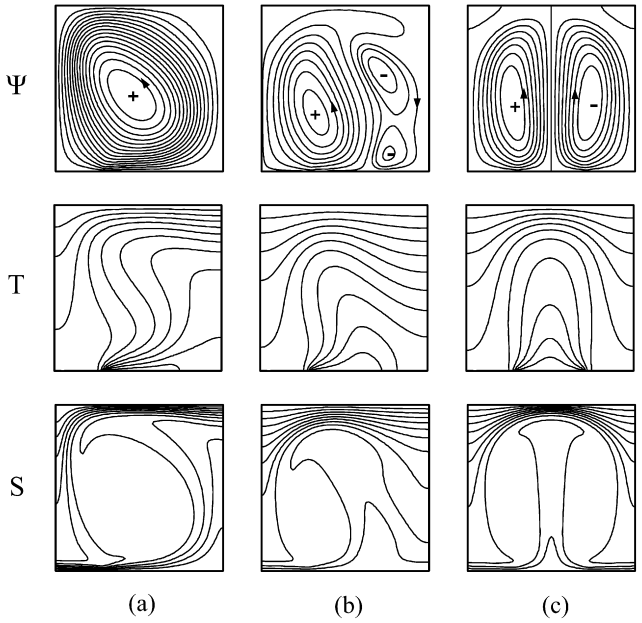

Fig. 4. Streamlines, isotherms and concentration lines illustrating the transition from unicellular to bicellular flow structures for $B_T = 0.4$, $\delta_T = 0$ and (a) $\varphi = -0.30$, (b) $\varphi = -0.50$ and (c) $\varphi = -0.53$.

φ is decreased up to $\varphi = -0.50$ Fig. 4(b) indicates the occurrence of a small eddy, located near the right-hand side wall, and rotating clockwise. Upon decreasing φ only from -0.50 to -0.53, Fig. 4(c) shows the occurrence of a bicellular natural flow circulation. The two symmetrical small counterrotating eddies, located near the upper corners of the cavity, result from the fact that the fluid is almost stagnant in that area, as it can be observed from the isotherms and concentration lines. The third branch reported in Fig. 3(a) corresponds to the bicellular antinatural convection mode. Upon decreasing φ below zero it is found that this type of solution is possible down to $\varphi = -0.17$ where the solution bifurcates towards the upper (lower) anticlockwise (clockwise) unicellular branch. The evolution of the flow structure during this transition is depicted in Fig. 5 for different time t. Thus, starting with a bicellular antinatural flow pattern at time $t = 0$, Fig. 5(a), the formation of a small anticlockwise cell occurs at time $t = 5.8$, in the vicinity of the left lower corner of the cavity, Fig. 5(b). As time increases, the intensity and strength of this small cell become stronger and eventually merge with the left hand side anticlockwise cell. To accommodate the newly formed large cell, the size and strength of the original clockwise cell is considerably reduced as depicted in Fig. 5(c). Finally, this mechanism leads to the formation of a single anticlockwise cell structure as shown in Fig. 5(d) for $t = 8.5$. Loss of stability of the bicellular antinatural convection mode to decreasing buoyancy ratio φ is thus by exchange of stability to the unicellular stable case. In fact, as discussed in the past by Sen et al. [25], antinatural flows are stable only for a restricted of the governing parameters. It is noted that the transition from the bicellular antinatural flow configuration to the unicellular structure results from the initial conditions imposes. Thus, upon using the rest state as initial conditions, the numerical results (not presented here) indicate the occurrence of a single steady state cell structure. A Hopf's bifurcation was also observed to occur for sufficiently large values of φ for the bicellular natural flow structure branch Fig. 3(a). The intensity of the resulting oscillating flow depends not only of the value of buoyancy ratio φ but also on that of the normalized porosity of the porous medium ε. Thus as illustrated in Fig. 6(a) at $\varphi \simeq 1.43$ and $\varepsilon = 1$, the flow starts to be periodically oscillating. However, as the value of ε is made smaller the strength of convection is considerably reduced such that the flow becomes steady when $\varepsilon = 0.6$. Upon increasing φ Figs. 6(b) and 6(c) show that, for $\varepsilon = 1$, the flow becomes progressively chaotic.

The numerical results presented in Fig. 3(a), for the case $Le = 10$, were obtained for $Le = 5$ in order to investigate the

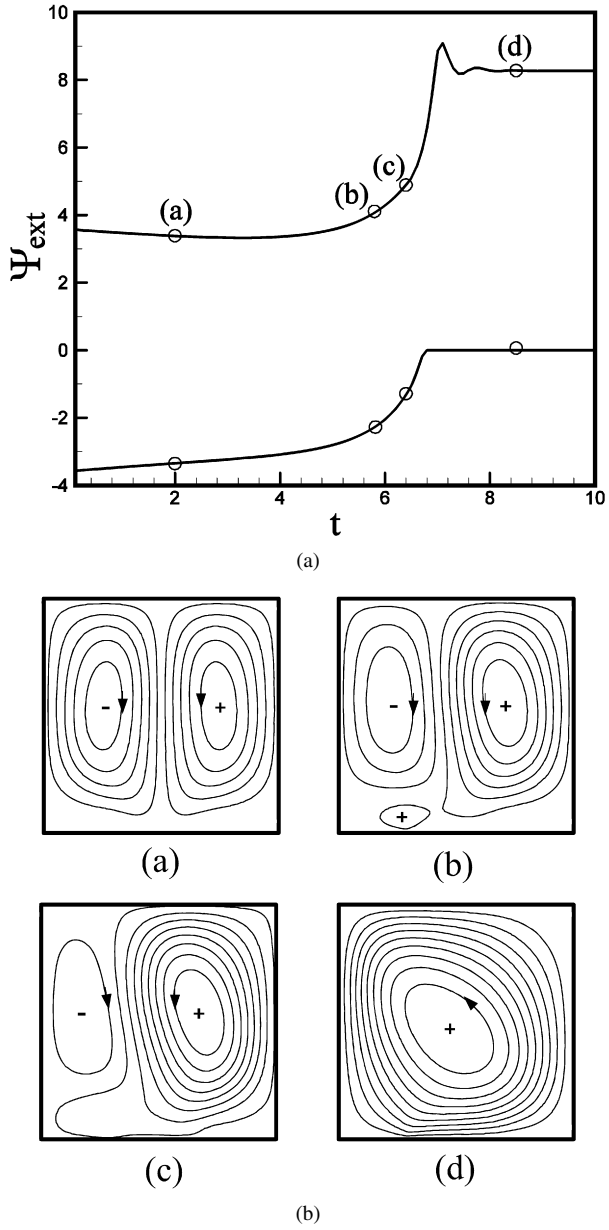

Fig. 5. Selected streamlines, isotherms and concentration lines obtained for $B_T = 0.4$, $\delta_T = 0$, $\varphi = -0.18$ and for (a) $t = 2$, (b) $t = 5.8$, (c) $t = 6.4$ and (d) $t = 8.5$.

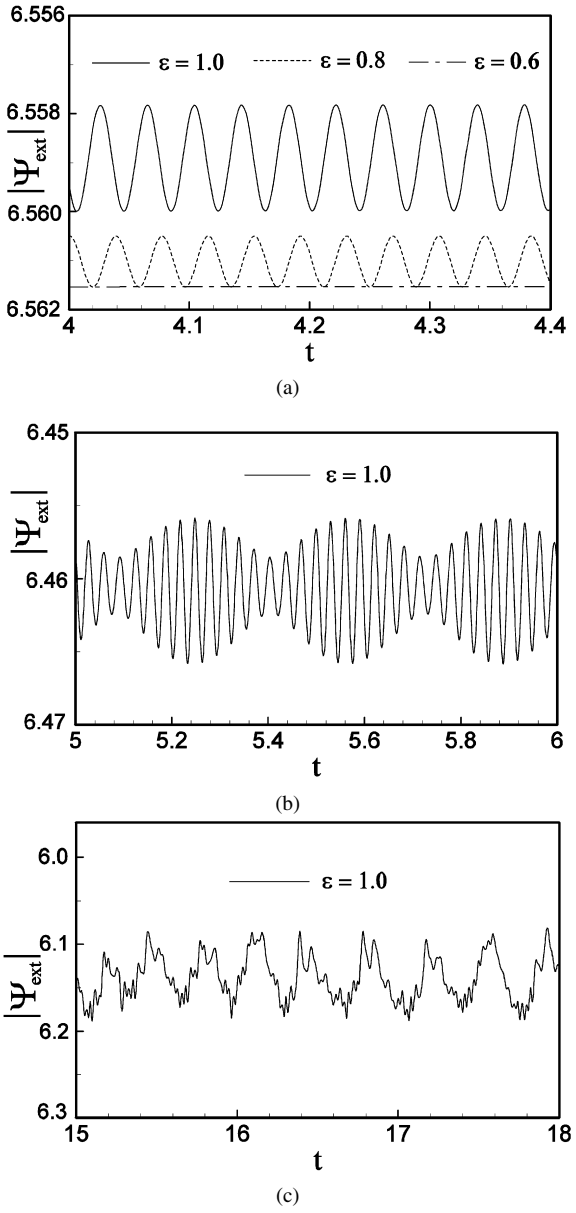

Fig. 6. The history of flow intensity $|\Psi_{ext}|$ for (a) $\varphi = 1.44$, (b) $\varphi = 1.47$ and (c) $\varphi = 1.55$.

influence of this parameter on the present problem. The resulting curves, Fig. 7, indicate that both results are qualitatively similar. However, the bifurcation of the bicellular antinatural branch, for $\varphi > 0$, is observed to be quite different. Thus, in Fig. 3(a), at $\varphi = 0.18$ the bicellular antinatural branch bifurcates towards the upper unicellular flow pattern. However, when $Le = 5$, Fig. 7 indicates that a steady antinatural bicellular solution is possible up to $\varphi = 0.15$ above which the flow pattern is found to be oscillating periodically in time. This unsteady regime is maintained up to $\varphi = 0.45$ where a transition towards the bicellular natural convective flow (and not the unicellular) occurs.

Fig. 8(a) shows the effect of φ on the maximum and minimum streamfunction Ψ_{max} and Ψ_{min}, respectively, in the case of a positive eccentricity of the heated element ($\delta_T = 0.15$). Here also, all the curves presented in the graph were started with the results presented in Figs. 2(b), 2(e) and 2(f), for $\varphi = 0$. Upon increasing φ from 0 to 1.36, and decreasing φ from 0 to -1.5, step by step using the previous result as initial conditions, the resulting solutions follow the hysteresis loops indicated by arrows. The upper curve corresponds to a unicellular natural counterclockwise circulation. Upon decreasing the value of φ it is observed that, as expected, the strength of convection is considerably reduced since the stabilizing influence of the solutal gradients is enhanced. Thus, as indicated by Figs. 8(b) and 8(c) the rest state ($Nu \to 1$, $Sh \to 1$) is almost reached for $\varphi \leqslant -0.96$. On the other hand the flow intensity and heat and mass transfer are promoted upon increasing φ above zero. This follows from the fact that for $\varphi > 0$ both the thermal and solutal gradients are destabilizing. The unicellular natural circulation

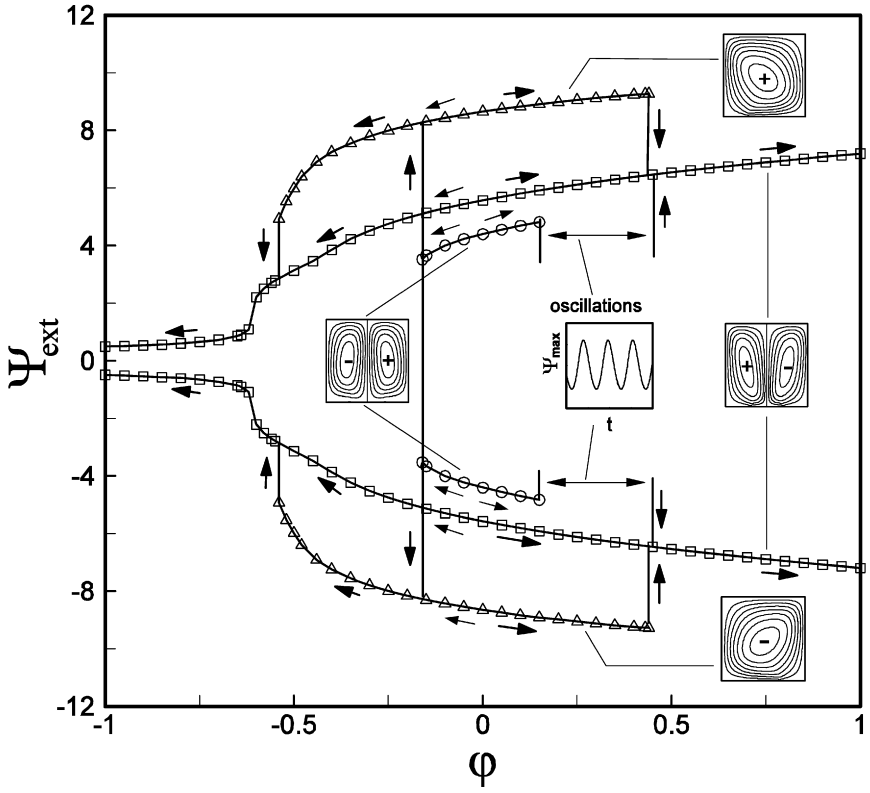

Fig. 7. Effect of buoyancy ratio φ on Ψ_{ext} for $B_T = 0.4$, $\delta_T = 0$ and $Le = 5$; △: 1 cell, □: 2 natural cells, ○: 2 antinatural cells.

can be maintained up to $\varphi \simeq 0.44$ where the flow bifurcates toward the bicellular natural branch. Finally, the lower branch in Fig. 8(a) corresponds to the unicellular clockwise antinatural branch. The range of extend of this flow structure is relatively small $-0.25 \leqslant \varphi \leqslant 0.47$ since the solution bifurcates toward the bicellular natural branch for other values of φ. Upon decreasing the value of φ below zero it is found that the bicellular antinatural flow can be maintained down to $\varphi = -0.26$ where the solution bifurcates toward the unicellular natural flow. Upon increasing the value of φ above zero the occurrence of a small clockwise eddy in the lower left corner of the cavity was observed at $\varphi = 0.85$. Above the value $\varphi = 1.36$ the numerical results indicate the existence of an oscillatory flow.

Figs. 9(a)–(d) illustrate the effect of the dimensionless length of heat source B_T on $|\Psi_{\text{ext}}|$. This problem has been investigated in the past (see for instance Mamou and Vasseur [10]) for the particular case $B_T = 1$, i.e. when the cavity is fully heated and salted from bottom. This situation corresponds to a classical Bénard situation for which it is well known that convection is possible only above a critical Rayleigh number R_{TC}. For $\varphi > 0$, i.e. when both the thermal and solutal gradients are destabilizing it was demonstrated by Nield [4], on the basis of the linear stability theory, that the supercritical Rayleigh number for the onset of unicellular motion is given by $Ra_{TC}^{\text{sup}} = 4\pi^2/(1 + \varphi Le)$. Thus, $Ra_{TC}^{\text{sup}} = 7.89$ when $\varphi = 0.4$ and $Ra_{TC}^{\text{sup}} = 6.58$ when $\varphi = 0.5$ such that unicellular convection is possible in Figs. 9(a) and 9(b) when $B_T = 1$, since the numerical results were obtained for a Rayleigh $R_T = 200$, i.e. well above the critical values for the onset of motion. Upon decreasing the value of B_T and using the last numerical solution as initial conditions the resulting curve, obtained for $\varphi = 0.4$, is depicted in Fig. 9(a). Naturally, the intensity of $|\Psi_{\text{ext}}|$ is found to decrease with B_T. For $B_T = 1$ and appropriate initial conditions the two cells structure is also possible, the sense of rotation of the two counterrotating eddies being induced by the initial conditions. Upon decreasing the value of B_T, two branches are obtained. The upper one corresponds to the bicellular natural flow for which the fluid is ascendant above the heated element. The other one, corresponding to the antinatural bicellular flow pattern, can be maintained down to $B_T = 0.45$, where the flow bifurcates toward the upper unicellular branch. Upon increasing φ from 0.4 to 0.5 yields the bifurcation curves presented in Fig. 9(b). It is noted that the upper unicellular flow structure is possible only down to $B_T = 0.95$, below which the flow pattern is found to be oscillating. The results obtained for $B_T = 0.925$ are depicted in Fig. 10, in terms of Ψ_{ext} versus time t, and the flow is observed to be periodically oscillating. Thus at $t = 29.60$ Fig. 10(a) shows that the flow pattern consists in a large counterclockwise cell and two small clockwise eddies located at the top right corner and bottom left corner. At time $t = 29.77$ the two small eddies have increased their size such that at $t = 30.04$ they have almost merged to occupy a large part of the cavity (Fig. 10(b)). This results in the formation of two counterclockwise cells in the upper left corner and lower right corner of the cavity as depicted in Fig. 10(c). At time $t = 30.74$ Fig. 10(d) shows that these two eddies have merged again to form a large counterclockwise cell. The whole process is repeated during each time period ($\tau = 2.60$). At $B_T = 0.75$,

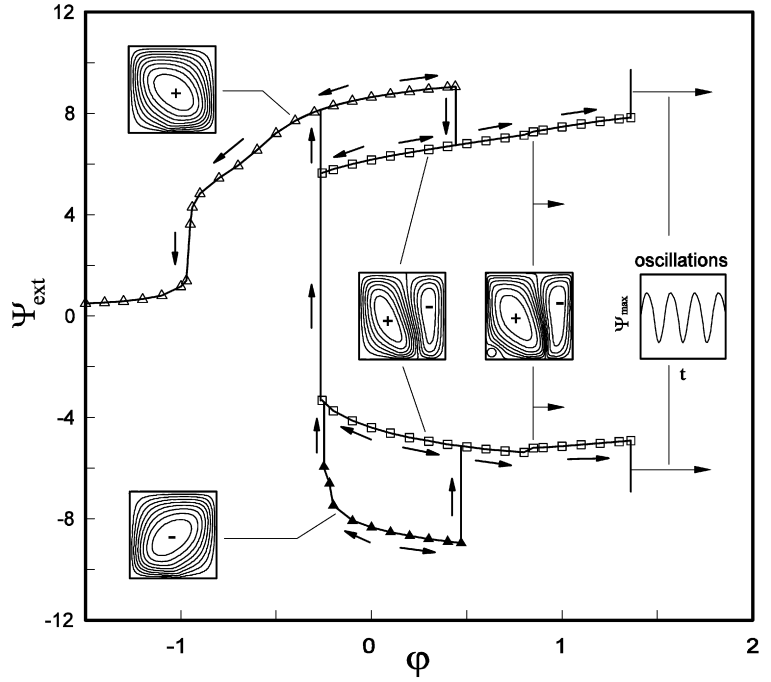

(a)

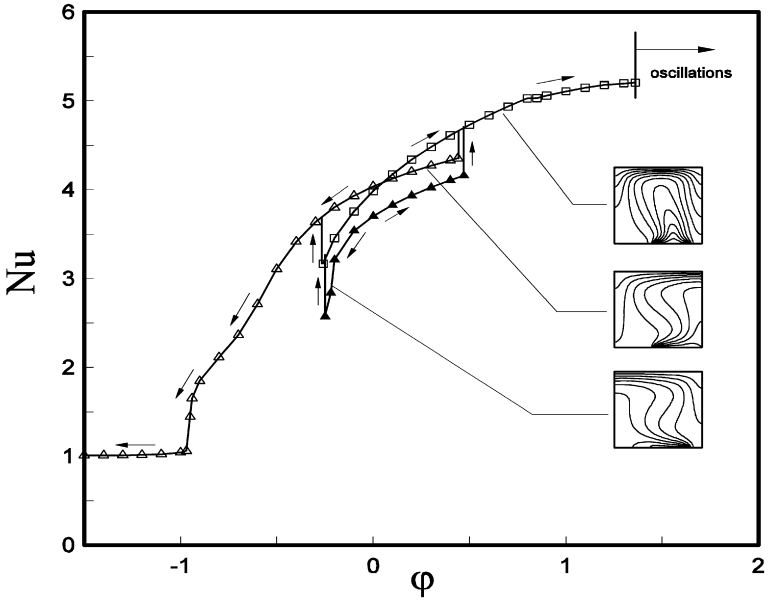

(b)

Fig. 8. Effect of buoyancy ratio φ on (a) Ψ_{ext}, (b) *Nu*, (c) *Sh*, for $B_T = 0.4$, $\delta_T = 0.15$; △: 1 natural cell, ▲: 1 antinatural cell, □: 2 natural cells, ○: 2 antinatural cells.

Fig. 9(b) indicates that the unsteady flow regime bifurcates toward the bicellular natural flow structure. On the other hand, the antinatural bicellular flow structure can be maintained down to $B_T = 0.475$, before bifurcating toward the bicellular natural branch. For $\varphi < 0$, i.e. when the thermal gradient are destabilizing while the solutal one stabilizing, the onset of motion occurs through a subcritical Rayleigh number [10]. For $\varphi = -0.4$, Fig. 9(c) shows that the solution is qualitatively similar to the results obtained in Fig. 9(a), for $\varphi = 0.4$. However, it is observed from Fig. 9(d) that for $\varphi = -0.5$ a symmetrical one mode cell solution does not exist. However, as it will be discussed at the end of this section a unicellular nonsymmetric flow pattern is possible.

Fig. 11(a) illustrates the effect of φ on Ψ_{ext} for the case of a cavity fully heated from bottom ($B_T = 1$). Starting with appropriate initial conditions a unicellular flow is obtained, for $\varphi = -0.4$, as depicted in the graph. Upon decreasing the value of φ it is observed that this flow configuration is maintained down to $\varphi = -0.44$ where the solution bifurcates toward a new configuration where the flow decreases in intensity and loses its spatial symmetry. As reported in Fig. 11(a), the cell is found to be shifted to the right while an almost quiescent flow ex-

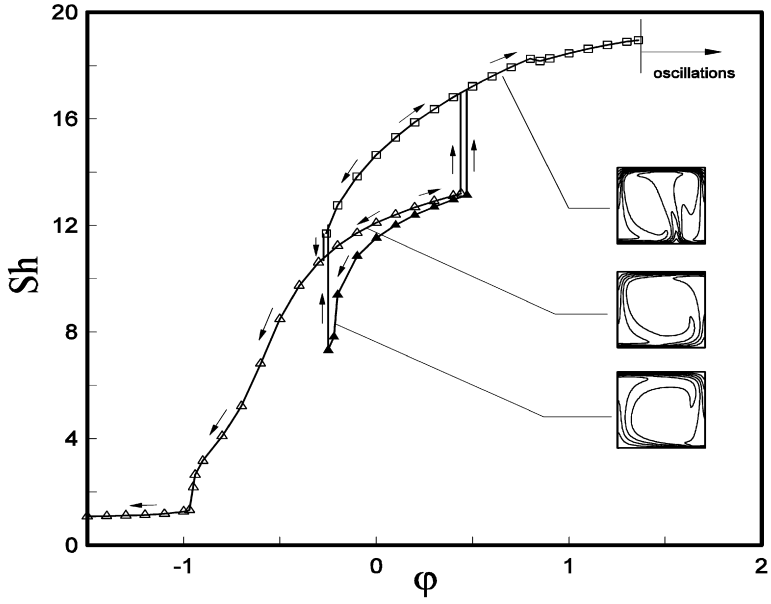

(c)

Fig. 8. (Continued).

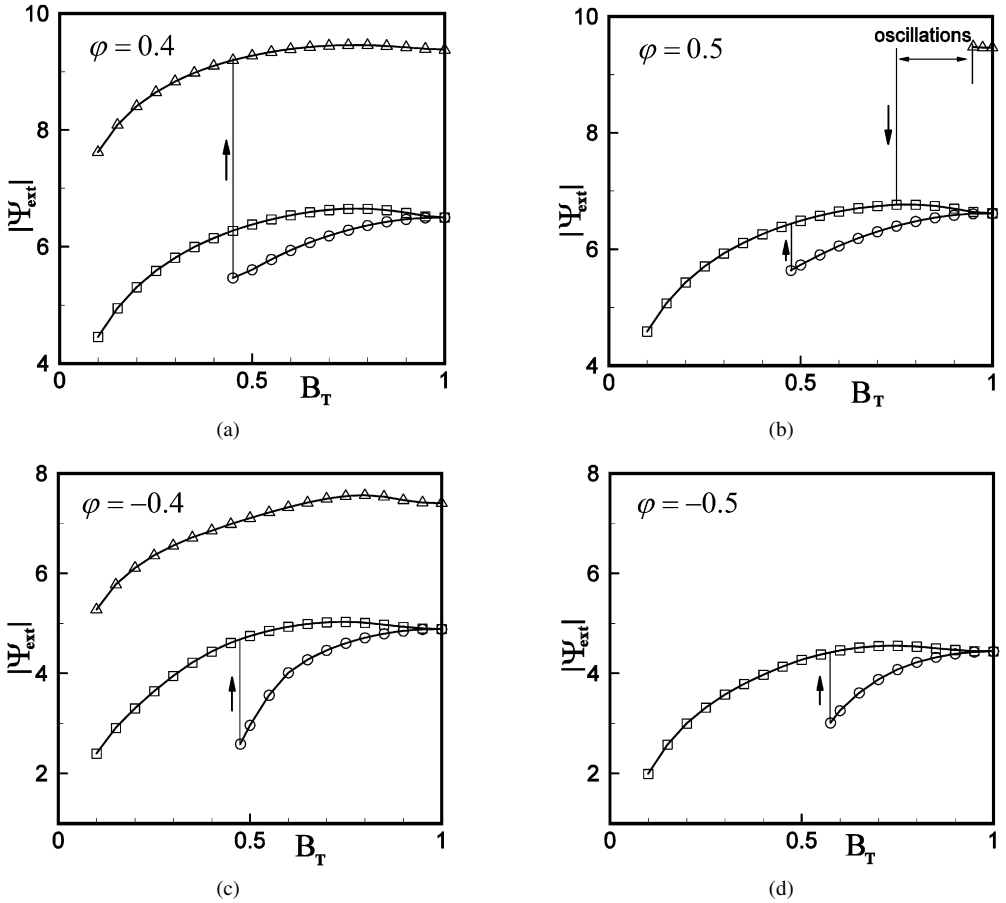

(a) (b) (c) (d)

Fig. 9. Effect of dimensionless length of heat source B_T on Ψ_{ext} for $\delta_T = 0$ (a) $\varphi = 0.4$, (b) $\varphi = 0.5$, (c) $\varphi = -0.4$, (d) $\varphi = -0.5$; △: 1 natural cell, □: 2 natural cells, ○: 2 antinatural cells.

ists in the left part of the container. This branch can be maintained down to $\varphi = -0.51$ where the rest state prevails as the value of φ is further decreased. The effect of the dimensionless length of the heated element B_T on Ψ_{ext} is depicted in Fig. 11(b). In addition of the natural and antinatural bicellular flow structures discussed in Fig. 9(d) the unicellular flow

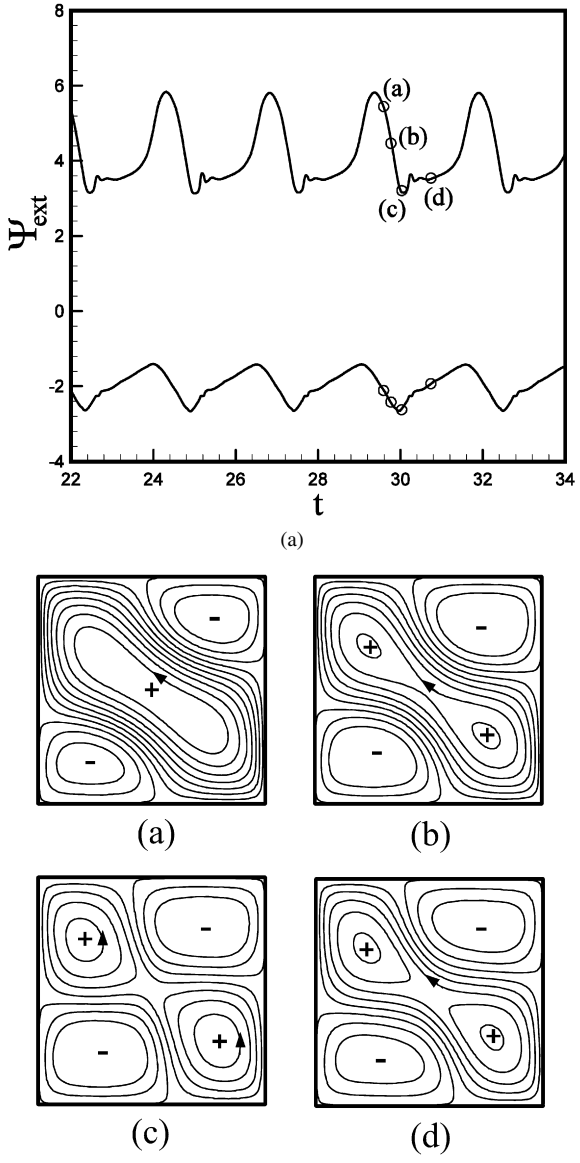

Fig. 10. The history of flow intensity Ψ_{ext} for $\varphi = 0.5$, $B_T = 0.925$ and $\delta_T = 0$; (a) $t = 29.60$, (b) $t = 29.77$, (c) $t = 30.04$, and (d) $t = 30.74$.

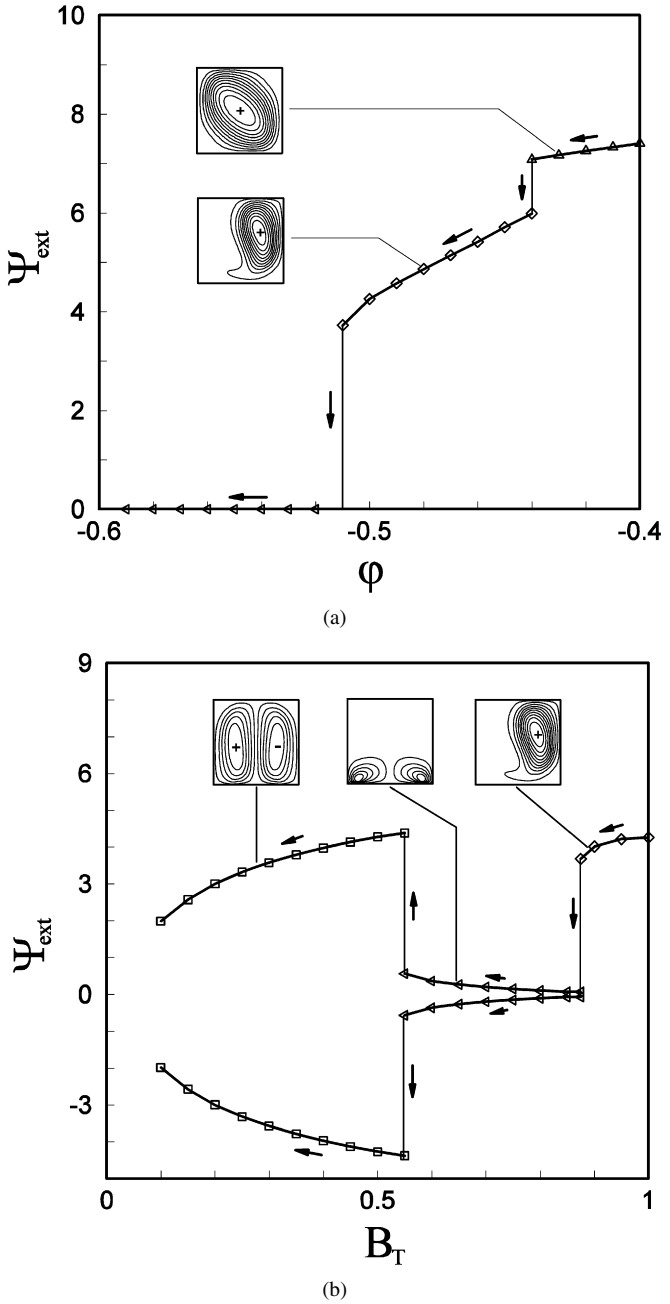

Fig. 11. Flow intensity Ψ_{ext} as a function of (a) φ for $B_T = 1$ and (b) B_T for $\varphi = -0.5$; △: 1 natural cell, □: 2 natural cells, ◇: 1 unsymmetrical cell, ◁: rest state.

regime reported in Fig. 11(a) for $\varphi = -0.5$ is also possible. Thus starting with this solution, as initial conditions, for $B_T = 1$ yields the asymmetric flow pattern discussed above. Upon decreasing the value of B_T this solution is maintained down to $B_T = 0.88$ for which the rest state is obtained. However, as the value of B_T is further decreased the appearance of two small eddies, in the bottom corners of the cavity is observed. The size and the intensity of these cells increase progressively, as the value of B_T is reduced. At $B_T = 0.55$ the flow pattern bifurcates to a symmetrical bicellular configuration. The intensity of the flow circulation decreased as the value of B_T is further reduced.

The existence of tricellular flows in square enclosure has been reported in the past by many authors (see for instance Mamou et al. [24]). In the present problem, upon starting the numerical procedure with appropriate boundary condition, it was found that such flow structures could be maintained for a given range of the governing parameters. Fig. 12(a) illustrates the effect of φ on $|\Psi_{ext}|$ for the case of a cavity fully heated from the bottom ($B_T = 1$). Upon decreasing the value of φ the results indicate that this configuration is maintained down to $\varphi = -0.17$ where the flow bifurcates toward a bicellular natural circulation. The effect of the dimensionless length of the heated element on the tricellular pattern is exemplified in Fig. 12(b). It is observed that this flow configuration can be sustained down to $B_T = 0.65$, below which the bicellular flow configuration is recovered.

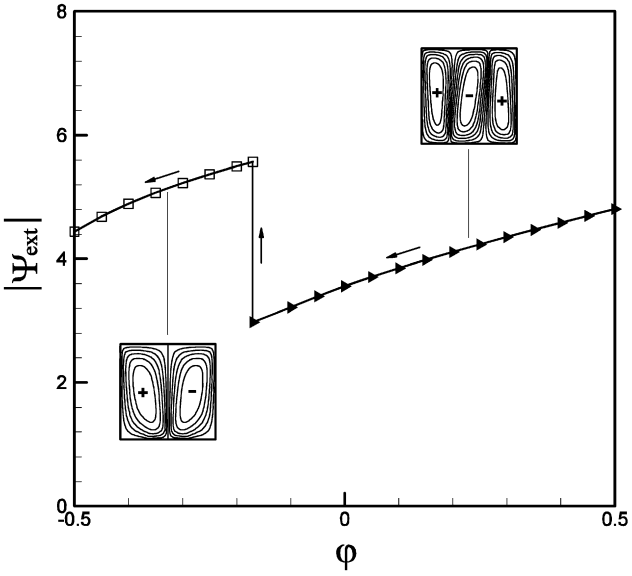

(a)

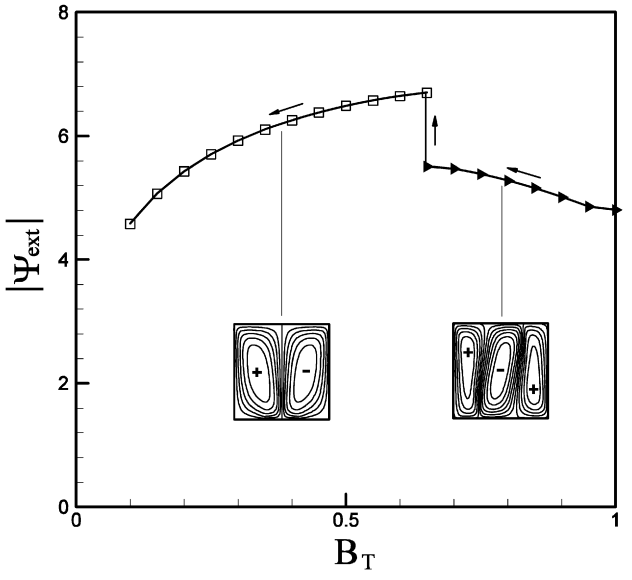

(b)

Fig. 12. Flow intensity $|\Psi_{ext}|$ as a function of (a) φ for $B_T = 1$ and (b) B_T for $\varphi = -0.5$; □: 2 natural cells, ►: 3 cells.

5. Conclusions

In the present investigation, the results of a numerical study of double diffusive convection in a two-dimensional square porous enclosure, salted and partially heated from below, are presented. The existence of a multiplicity of steady state solutions for the present numerical problem has been demonstrated numerically through the use of appropriate initial perturbations. The main conclusions of the present analysis are as follows

1° Centrally located heated element ($\delta_T = 0$): it was found that both unicellular and bicellular symmetrical circulations are possible. When a single cell is involved the flow circulation may be clockwise or counterclockwise, one being the mirror image of the other. This flow pattern can be reached only through appropriate initial conditions. When two cells are involved two different solutions, termed natural and antinatural, are possible. The first one, corresponding to the case where the fluid motion above the heated element is upward, can be obtained starting from the rest condition ($\Psi = 0$). The second one, for which the fluid motion above the heat source is downward, can be obtained only by using appropriate initial conditions. The natural solution corresponds to the maximum flow intensity and heat and mass transfers. For a given set of the governing parameters it has been demonstrated that up to three different solutions, corresponding to the above flow structures, are possible. The range of existence of these solutions depends strongly upon the governing parameters considered. Also, in the present study, the existence of tricellular flows has been observed for a given range of the governing parameters.

2° Eccentrically located heated element ($\delta_T > 0$): for this situation the unicellular anticlockwise (clockwise) circulation corresponds to a natural (antinatural) flow, this latter being up (down) over the heated element. Also, the numerical results indicate the existence of a bicellular flow structure, the flow above the heated element being upward. Thus for this situation, up to three different solutions are also possible for a given set of the governing parameters.

In addition to the above flow configurations, various phenomena have been observed such as oscillatory periodic and aperiodic flow structures. Also, the existence of nonsymmetric unicellular flows, has been demonstrated.

References

[1] S. Ostrach, Natural convection with combined driving forces, Phys. Chem. Hydrodyn. 1 (1980) 233–247.

[2] R. Viskanta, T.L. Bergman, F.P. Incropera, Double diffusive natural convection, in: Natural Convection Fundamentals and Applications, Hemisphere, 1985, pp. 1075–1099.

[3] A. Nield, A. Bejan, Convection in Porous Media, second edition, Springer, 1999.

[4] D.A. Nield, Onset of thermohaline convection in a porous medium, Water Resources Res. 4 (1968) 553–560.

[5] J.W. Taunton, E.N. Lightfoot, T. Green, Thermohaline instability and salt fingers in a porous medium, Phys. Fluids 15 (1972) 748–753.

[6] N. Rudraiah, P.K. Srimani, R. Friedrich, Finite amplitude convection in a two-component fluid saturated porous layer, Int. J. Heat Mass Transfer 25 (1981) 715–722.

[7] D. Poulikakos, Double-diffusive convection in horizontal sparsely packed porous layer, Int. J. Heat Mass Transfer 13 (1986) 587–598.

[8] M.E. Taslim, U. Narusaw, Binary fluid composition and double diffusive convection in a porous medium, J. Heat Transfer 108 (1986) 221–224.

[9] V. Trevisan, A. Bejan, Mass and heat transfer by high Rayleigh number convection in a porous medium heated from below, Int. J. Heat Mass Transfer 30 (1987) 2341–2356.

[10] M. Mamou, P. Vasseur, Thermosolutal bifurcation phenomena in porous enclosures subject to vertical temperature and concentration gradients, J. Fluid Mech. 395 (1999) 61–87.

[11] O. Sovran, M. Charrier-Mojtabi, A. Motjabi, Naissance de la convection thermo-solutale en couche poreuse infinie avec effet Soret, Mécanique des fluides 329 (2001) 287–293.
[12] A. Bahloul, N. Boutana, P. Vasseur, Double-diffusive and Soret-induced convection in a shallow horizontal porous layer, J. Fluid Mech. 491 (2003) 325–352.
[13] J.W. Elder, Steady free convection in a porous medium heated from below, J. Fluid Mech. 47 (1967) 29–48.
[14] J.W. Elder, Transient convection in a porous medium, J. Fluid Mech. 47 (1967) 609–623.
[15] G. El-Khatib, V. Prasad, Effects of stratification on thermal convection in horizontal porous layer with localized heating from below, J. Heat Transfer 109 (1987) 683–687.
[16] L. Robillard, C. H Wang, P. Vasseur, Multiple steady states in confined porous medium with localized heating from below, Numer. Heat Transfer 13 (1988) 91–110.
[17] M. Bourich, M. Hasnaoui, A. Amahmid, Double-diffusive natural convection in a porous enclosure partially heated from below and differentially salted, Int. J. Heat Fluid Flow 25 (2004) 1034–1046.
[18] D. Liu, F. Y Zhao, G.F. Tang, Thermosolutal convection in saturated porous enclosure with concentrated energy and solute sources, Energy Conversion & Management 49 (2008) 16–31.
[19] F.Y. Zhao, D. Liu, G.F. Tang, Natural convection in a porous enclosure with partial heating and salting element, Int. J. Thermal Sci. 47 (2008) 569–583.
[20] F.Y. Zhao, D. Liu, G.F. Tang, Multiple steady flows in confined gaseous double diffusion with discrete thermosolutale sources, Phys. Fluids 19 (2007) 2889–2904.
[21] F.Y. Zhao, D. Liu, G.F. Tang, Free convection from one thermal and solute source in a confined porous medium, Transport Porous Media 70 (2007) 407–425.
[22] S.R. De Groot, P. Mazur, Non Equilibrium Thermodynamics, North-Holland, Amsterdam, 1962, Wiley, New York.
[23] S. Patankar, Numerical Heat Transfer and Fluid Flow, Hemisphere, Washington, DC, 1980.
[24] M. Mamou, P. Vasseur, M. Hasnaoui, On numerical stability analysis of double-diffusive convection in confined enclosures, J. Fluid Mech. 433 (2001) 209–250.
[25] M. Sen, P. Vasseur, L. Robillard, Multiple steady states for unicellular natural convection in an inclined porous layer, Int. J. Heat Mass Transfer 30 (1987) 2097–2113.
[26] B. Goyeau, J.P. Songbe, D. Gobin, Numerical study of double-diffusive natural convection in porous cavity using the Darcy–Brinkman formulation, Int. J. Heat Mass Transfer 39 (1996) 1363–1378.